Near-wall turbulent fluctuations in the absence of wide outer motions

Yongyun Hwang

J. Fluid Mech. (2013), *vol.* 723, *pp.* 264–288.
doi:10.1017/jfm.2013.133

Near-wall turbulent fluctuations in the absence of wide outer motions

Yongyun Hwang†

Laboratoire d'Hydrodynamique (LadHyX), CNRS École Polytechnique, 91128 Palaiseau, France

(Received 22 August 2012; revised 27 February 2013; accepted 28 February 2013;
first published online 16 April 2013)

Numerical experiments that remove turbulent motions wider than $\lambda_z^+ \simeq 100$ are carried out up to $Re_\tau = 660$ in a turbulent channel. The artificial removal of the wide outer turbulence is conducted with spanwise minimal computational domains and an explicit filter that effectively removes spanwise uniform eddies. The mean velocity profile of the remaining motions shows very good agreement with that of the full simulation below $y^+ \simeq 40$, and the near-wall peaks of the streamwise velocity fluctuation scale very well in the inner units and remain almost constant at all the Reynolds numbers considered. The self-sustaining motions narrower than $\lambda_z^+ \simeq 100$ generate smaller turbulent skin friction than full turbulent motions, and their contribution to turbulent skin friction gradually decays with the Reynolds number. This finding suggests that the role of the removed outer structures becomes increasingly important with the Reynolds number; thus one should aim to control the large scales for turbulent drag reduction at high Reynolds numbers. In the near-wall region, the streamwise and spanwise velocity fluctuations of the motions of $\lambda_z^+ \leqslant 100$ reveal significant lack of energy at long streamwise lengths compared to those of the full simulation. In contrast, the losses of the wall-normal velocity and the Reynolds stress are not as large as those of these two variables. This implies that the streamwise and spanwise velocities of the removed motions penetrate deep into the near-wall region, while the wall-normal velocity and the Reynolds stress do not.

Key words: turbulence simulation, turbulent boundary layers, turbulent flows

1. Introduction

The near-wall region of wall-bounded turbulent flows has been intensively studied for the last two decades. The near-wall process involves prominent coherent structures such as streaks and streamwise vortices (Kline *et al.* 1967; Smith & Metzler 1983; Kim, Moin & Moser 1987; Jeong *et al.* 1997). Interaction between these structures plays an important role in the near-wall turbulence and skin friction generation. The streamwise vortices lead to strong amplification of the streaks via the 'lift-up' effect, a process that transfers the energy of mean shear to turbulent fluctuations (Landahl 1990; Butler & Farrell 1993; del Álamo & Jiménez 2006; Cossu, Pujals & Depardon 2009; Pujals *et al.* 2009; Hwang & Cossu 2010*b*; Willis, Hwang & Cossu 2010).

† Present address: Department of Applied Mathematics and Theoretical Physics, University of Cambridge, Cambridge CB3 0WA, UK. Email address for correspondence: Y.Hwang@damtp.cam.ac.uk

The amplified streaks then undergo rapid oscillation due to secondary instability or transient growth, which, in turn, regenerates the streamwise vortices via nonlinear mechanisms (Hamilton, Kim & Waleffe 1995; Waleffe 1997; Schoppa & Hussain 2002). Recent effort based on dynamical system approaches has shown that the near-wall turbulence in small computational boxes can be characterized by several exact solutions, such as unstable travelling waves and periodic orbits, which form a skeleton of the solution trajectory in phase space (see e.g. Waleffe 1998, 2001, 2003; Faisst & Eckhardt 2003; Wedin & Kerswell 2004; Jiménez *et al.* 2005; Gibson, Halcrow & Cvitanovic 2008).

One of the most important features in the near-wall region is probably that the process is essentially independent of the outer turbulence. Early numerical experiments have shown that the near-wall turbulence is maintained in small computational boxes, which do not provide enough space for large eddies in the outer region (Jiménez & Moin 1991; Hamilton *et al.* 1995). The near-wall turbulence is sustained even under more severe conditions where the outer turbulence is artificially damped out (Jiménez & Pinelli 1999; Jiménez, del Álamo & Flores 2004). The independent characteristics of the near-wall region have been thought to be a core mechanism of near-wall turbulence production, although a growing body of recent evidence has proposed that the near-wall region is largely influenced by the energetic outer structures, particularly at high Reynolds numbers (De Graaff & Eaton 2000; del Álamo & Jiménez 2003; Hutchins & Marusic 2007; Mathis, Hutchins & Marusic 2009). For further details on recent developments in high-Reynolds-number wall turbulence research, the reader may refer to a recent review by Marusic *et al.* (2010*b*).

The near-wall coherent structures have been well characterized with their spanwise length scale (or spacing) $\lambda_z^+ \simeq 100$ (Kline *et al.* 1967; Smith & Metzler 1983; Kim *et al.* 1987). As the observation point moves from the near-wall region to the outer region, the spanwise length scale undergoes gradual growth. In the logarithmic layer, the growth is roughly proportional to the distance of the observation point from the wall (Tomkins & Adrian 2003; del Álamo *et al.* 2004; Ganapathisubramani *et al.* 2005). The growth stops when the spanwise length scale reaches $\lambda_z \simeq O(1\delta)$ (where δ is the outer length scale), which represents the spanwise spacing of the outer coherent structures such as large-scale and very-large-scale motions (del Álamo & Jiménez 2003; del Álamo *et al.* 2004; Tomkins & Adrian 2005; Hutchins & Marusic 2007). The spanwise length scale growth from the near-wall to the outer scales is an important feature of wall turbulence, because it directly supports early seminal theoretical works in which the eddies in wall-bounded turbulent flows are assumed to consist of a hierarchy of 'attached' eddies (Townsend 1976; Perry & Chong 1982; Perry, Henbest & Chong 1986). It was initially proposed that the growth of the eddy size may originate from pairing or growth of the hairpin vortices in the near-wall region (Perry *et al.* 1986; Tomkins & Adrian 2003; Adrian 2007). However, recent theoretical and numerical investigations have revealed that the eddies at a given length scale are likely to bear their own sustaining mechanisms, which are essentially independent of those at other different length scales (del Álamo *et al.* 2006; Flores & Jiménez 2010; Hwang & Cossu 2010*b*,*c*, 2011; Park, Hwang & Cossu 2011).

Motivated by these recent observations, the question that we are essentially interested in here is this: 'What is the nature of turbulent fluctuation at a given spanwise length scale?' Since the spanwise length scale at a given wall-normal location roughly characterizes the size of the eddies at that location, we believe that the answer to this question would be able to unveil many important statistical and dynamical features of the hypothetical 'attached' eddies. As the first step, the present

study is aimed at understanding the nature of turbulent fluctuations narrower than $\lambda_z^+ \simeq 100$, the well-known spanwise spacing of the near-wall streaks and streamwise vortices (Kline *et al.* 1967; Smith & Metzler 1983; Kim *et al.* 1987). For this purpose, we design a numerical experiment that artificially removes turbulent fluctuations wider than $\lambda_z^+ \simeq 100$. Since near-wall turbulence narrower than $\lambda_z^+ \simeq 100$ is known to sustain in the absence of wide outer motions (Jiménez & Moin 1991; Jiménez & Pinelli 1999), we would expect that the fluctuations narrower than $\lambda_z^+ \simeq 100$ reasonably describe turbulent motions at least in the near-wall region. From this perspective, the present numerical experiment is in a similar context to the early investigations by Jiménez & Pinelli (1999) and Jiménez *et al.* (2004), where turbulence above a given wall-normal location is artificially damped out.

However, contrary to these studies, the present numerical experiment, which provides a filtering in the spanwise direction, allows the near-wall motions to develop naturally to the outer region almost without large-scale self-organization of the near-wall motions observed in Jiménez *et al.* (2004). Furthermore, we have found that the near-wall region with this type of filtering reveals very little outer-flow influence. These features enable us to examine several important questions associated with both the near-wall and outer turbulence: How do the near-wall turbulent fluctuations in the absence of wide outer turbulence scale with the Reynolds number? Do the near-wall streamwise velocity fluctuations in this case remain constant when they scale with the inner units? What is the contribution of the near-wall turbulence to skin-friction drag? Does it dominantly contribute to the skin friction even at sufficiently high Reynolds numbers, like at low Reynolds numbers? What wall-normal extent does the turbulence narrower than $\lambda_z^+ \simeq 100$ reach in the absence of the outer turbulence? Is it confined only to the near-wall region even in this case?

The objective of the present study is to answer the questions addressed above. The present paper is organized as follows. In § 2, we introduce details of the present numerical experiment, which has been carried out in a turbulent channel up to $Re_\tau = 660$. The results of the numerical experiment are then presented in § 3, and their discussions are given in § 4. In § 5, we summarize the present work and conclude with some remarks.

2. Numerical experiments

2.1. *Numerical methods*

We consider a flow over a turbulent channel with the fluid density ρ and the dynamic viscosity ν. The height of the channel is chosen as $2h$, and its upper and lower walls are respectively located at $y = 0$ and $2h$. We denote by x , y and z the streamwise, wall-normal and spanwise directions of the channel, respectively. The numerical experiments in the present study are carried out using a code for direct numerical simulation (DNS), which has been verified in our previous studies (Hwang & Cossu 2010*c*, 2011). In this code, the streamwise and spanwise directions are discretized using the Fourier series with 2/3 rule for dealiasing, and the wall-normal direction is discretized using the second-order central difference. The time integration is conducted semi-implicitly based on the fractional-step method (Kim & Moin 1985). All the terms with wall-normal derivatives are implicitly advanced with the second-order Crank–Nicolson method, while the rest of the terms are explicitly integrated with the third-order Runge–Kutta method. All the computations in the preset study are performed by imposing a constant mass flux across the channel. The detailed

Case	Re_m	Re_τ	Δ_x^+	Δ_z^+	L_x^+	L_z^+	$N_x \times N_y \times N_z$
$F180$	5600	178	17.4	5.8	3336	556	$192 \times 129 \times 96$
$S180$	6407	185	18.2	6.9	3488	111	$192 \times 129 \times 16$
$N180$	6407	190	18.6	7.1	3572	114	$192 \times 129 \times 16$
$L180$	6407	204	19.9	6.3	3837	204	$192 \times 129 \times 32$
$S410$	19333	418	11.4	6.8	4380	110	$384 \times 257 \times 16$
$N410$	19333	413	11.3	6.8	4328	108	$384 \times 257 \times 16$
$L410$	19333	490	10.3	6.1	3957	196	$384 \times 257 \times 32$
$S660$	43010	695	11.4	6.8	4365	109	$384 \times 257 \times 16$
$N660$	43010	660	10.8	6.5	4144	104	$384 \times 257 \times 16$
$L660$	43010	878	11.0	6.6	4214	211	$384 \times 385 \times 32$

TABLE 1. Simulation parameters in the present study. Here, $Re_\tau = u_\tau h/\nu$, with the friction velocity u_τ, and $Re_m = 2U_m h/\nu$, with the bulk velocity U_m. The filter (2.2) is applied to $N180$, $L180$, $N410$, $L410$, $N660$ and $L660$.

parameters of the simulations performed in the present study are summarized in table 1.

2.2. *Removal of motions wider than* $\lambda_z^+ \simeq 100$

Now, we design a numerical experiment that artificially removes turbulence wider than the spanwise wavelength $\lambda_z^+ \simeq 100$. From the given perspective, resolving structures wider than $\lambda_z^+ \simeq 100$ would not be necessary. Therefore, we consider spanwise domains as $L_z^+ \simeq 100$ (spanwise 'minimal' domain) while we choose reasonably long streamwise domains to resolve the long near-wall streaky structures ($L_x^+ \simeq 3500$–4500). This narrow and long computational domain is reminiscent of Toh & Itano (2005), where wide and short computational domains are considered to study the interaction between the near-wall and large-scale structures, though the scope of the present study is completely different from that study. Note that, even in these computational boxes, the spanwise discretization (Fourier–Galerkin method) allows the presence of turbulent structures wider than $L_z^+ \simeq 100$ because zero spanwise wavenumber ($k_z = 0$) still resolves the spanwise uniform eddies, i.e. two-dimensional eddies in the x–y plane. As we shall see in § 2.3, eddies of this type indeed appear in the narrow and long computational boxes. Therefore, an additional numerical strategy is complemented with the spanwise minimal domain to remove the spurious spanwise uniform eddies.

We start by rewriting the fractional-step method used in the present study, which practically consists of the following steps (Kim & Moin 1985):

$$\mathrm{LHS}_i \hat{u}_i^{k+1} = \mathrm{RHS}_i(u_i^k, p^k), \tag{2.1a}$$

$$\nabla^2 \phi^{k+1} = \mathrm{RHS}_\phi(\hat{u}_i^{k+1}), \tag{2.1b}$$

$$u_i^{k+1} = \hat{u}_i^{k+1} + C_u(\phi^{k+1}), \quad p^{k+1} = p^k + C_p(\phi^{k+1}), \tag{2.1c}$$

where (2.1*a*) is the discretized momentum equation, and (2.1*b*) and (2.1*c*) are the velocity and pressure correction procedures for the continuity. Here, k is the substep of the third-order Runge–Kutta method, u_i is the velocity in the i ($= x, y, z$) direction, p is the pressure, $\hat{u}_i$ is the pseudo-velocity and ϕ is the pseudo-pressure. The operator LHS_i indicates the left-hand side of the ith component of the discretized momentum

equation, while RHS_i and RHS_ϕ are the right-hand sides of the ith component of the momentum equation and the Poisson equation, respectively. The operators C_u and C_p are respectively the correction terms of the velocity and pressure for the continuity.

The removal of the spanwise uniform eddies from numerical solutions is conducted by explicitly imposing the following conditions on (2.1*a*) at each Runge–Kutta substep:

$$\widehat{\mathrm{RHS}}_x(y, k_x \neq 0, k_z = 0) = 0, \tag{2.2a}$$

$$\widehat{\mathrm{RHS}}_y(y, k_x \neq 0, k_z = 0) = 0, \tag{2.2b}$$

where $\widehat{\cdot}$ implies the Fourier-transformed state in the x and z directions. Here, (2.1*b*) and (2.1*c*) are not modified, so that the numerical solutions satisfy the continuity. For this reason, the numerical solution still contains small amounts of the spanwise uniform structures due to the unmodified equations (2.1*b*) and (2.1*c*). Also, it should be mentioned that the procedure (2.2) may affect the nonlinear dynamics of non-zero spanwise wavenumbers because it completely prevents the presence of nonlinear interactions between the $k_z = 2\pi n/L_z$ and $-2\pi n/L_z$ components (where $n = 1, \ldots, N_z/2$) of the streamwise and wall-normal velocities. However, as we shall see in the next section, the procedure (2.2) seems to effectively remove the non-physical spanwise uniform eddies and has only little influence on the statistics generated by motions narrower than $\lambda_z^+ \simeq 100$ (see also figure 2). Finally, it is worth pointing out that removal of the spanwise velocity by setting $\widehat{\mathrm{RHS}}_z(y, k_x \neq 0, k_z = 0) = 0$ along with (2.2) is intentionally avoided to minimize the effect of the filter on the motions of interest. Preliminary tests of the present numerical experiment (*S*180, *S*410 and *S*660) have revealed that the spanwise uniform components mainly consist of intense wall-normal velocity structures located near the channel centre (see also figures 1 and 2). Therefore, the filter (2.2) is designed to act mainly on the wall-normal velocity through $\widehat{\mathrm{RHS}}_y(y, k_x \neq 0, k_z = 0) = 0$, with a complementary setting $\widehat{\mathrm{RHS}}_x(y, k_x \neq 0, k_z = 0) = 0$. We note that the latter is aimed at numerically enhancing continuity for $k_z = 0$ in which the spanwise velocity does not play any role. The filter (2.2) therefore mainly acts on two-dimensional eddies populating the x–y plane.

2.3. *Preliminary test at* $Re_\tau \simeq 180$

We conduct a preliminary test of the designed numerical experiment at a low Reynolds number, $Re_\tau = u_\tau h/\nu \simeq 180$ (where u_τ is the friction velocity). We first perform a reference DNS with a sufficiently wide and long domain to verify the simulation code (*F*180 in table 1). Figure 1 shows its mean velocity profile and velocity fluctuations, which are in very good agreement with those by del Álamo *et al.* (2004). We then perform a simulation only with the spanwise minimal domain (*S*180 in table 1). The statistics in the near-wall region agree reasonably well with those of the full simulation, whereas they are quite different from those in the full simulation around the channel centre. The velocity fluctuations have non-negligibly large values near the channel centre even though the motions wider than $\lambda_z^+ \simeq 100$ are not resolved appropriately (figure 1*b–d*). In particular, the wall-normal velocity fluctuation is even larger than that of the full simulation near the channel centre (figure 1*c*). The increase of the wall-normal velocity fluctuation near the channel centre has not been observed in any of the previous minimal box experiments (Jiménez & Moin 1991; Jiménez & Pinelli 1999), implying that it is likely to be an artifact of the much longer computational domain in the present study. Now, the effect of the filtering (2.2) on the simulation with the spanwise minimal domain is studied (*N*180 in table 1). As

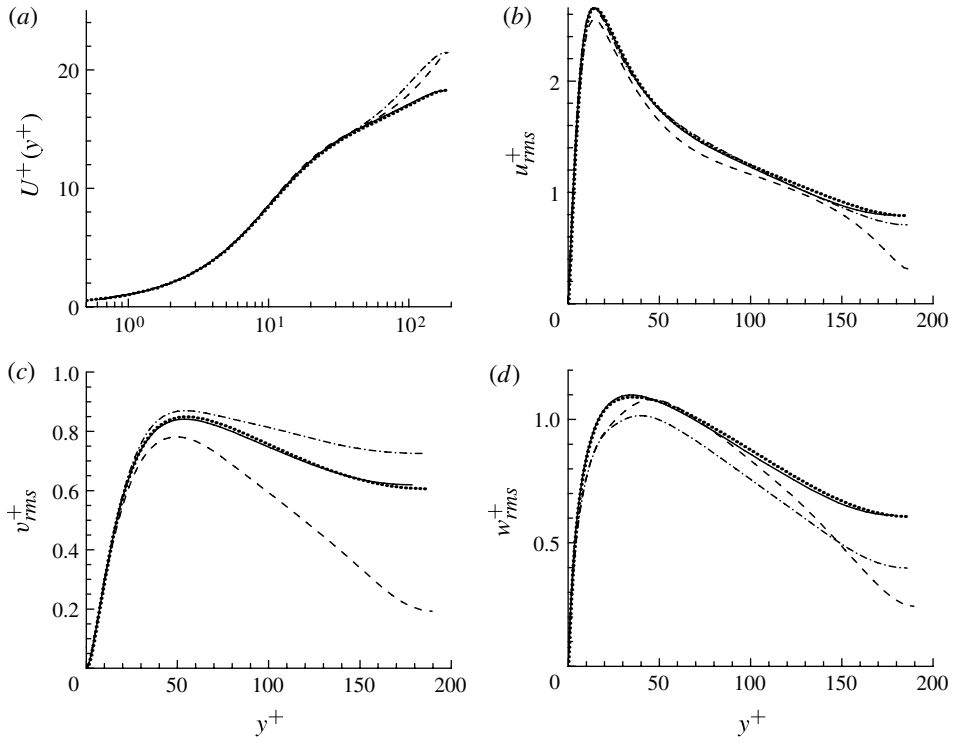

FIGURE 1. (*a*) Mean velocity profile $U^+(y^+)$ and turbulent velocity fluctuations (*b*) $u^+_{rms}(y^+)$, (*c*) $v^+_{rms}(y^+)$ and (*d*) $w^+_{rms}(y^+)$. Curves: ——, $F180$; · · · · · ·, DNS by del Álamo *et al.* (2004); — · — · —, $S180$ (spanwise minimal domain only); - - - -, $N180$ (spanwise minimal domain with the filtering (2.2)).

seen in the table 1, the filtering does not significantly change the friction Reynolds number. The mean velocity profile also shows good agreement with that of the full simulation below $y^+ \simeq 40$. The velocity fluctuations are also in reasonable agreement in the near-wall region, but they now tend to be smaller over the entire wall-normal domain (figure 1*b–d*). In particular, a substantial amount of turbulent kinetic energy is lacking near the channel centre, implying that the filtering (2.2) mainly damps out turbulent fluctuations at this location, which seem to be mainly resolved by zero spanwise wavenumber ($k_z = 0$).

One-dimensional spectra provide further details on the flow fields. For illustrative purposes, here we focus only on the effect of the spanwise minimal domain and the filtering (2.2) on the wall-normal velocity spectra, and a more comprehensive discussion on the spectra is deferred to § 3.3. Figure 2 shows the one-dimensional spectra of the wall-normal velocity. The spanwise spectra of the simulations only with the spanwise minimal domain ($S180$) and both with the minimal domain and with the filtering (2.2) ($N180$) agree reasonably well with those of the full simulation ($F180$) for $\lambda_z^+ \leqslant 100$, although they tend to carry a little more energy in the outer region than those of the full simulation (figure 2*a*). However, in the streamwise spectra, the reasonable agreement appears only in the near-wall region (figure 2*b*). The spectra of all three simulations for $y^+ \geqslant 50$ are remarkably different from each other, suggesting that the streamwise spectra at this location are mainly related to the structures wider

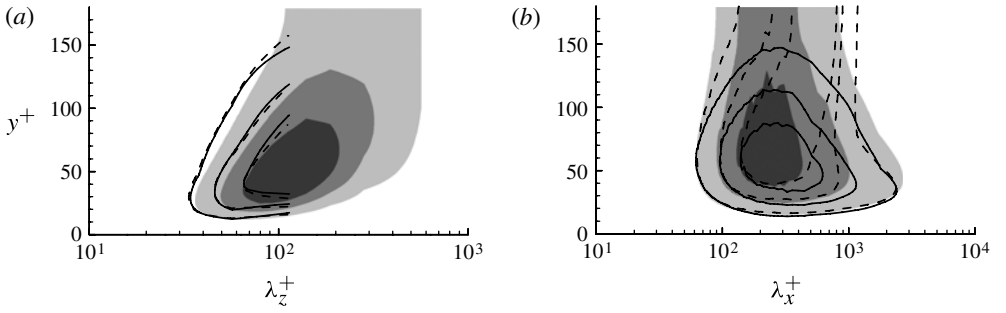

FIGURE 2. Premultiplied one-dimensional spectra of the wall-normal velocity: (*a*) spanwise and (*b*) streamwise spectra. Here: shaded, *F*180; dashed line, *S*180; solid line, *N*180. The contour labels are uniformly spaced from zero.

than $\lambda_z^+ \simeq 100$. In the simulation only with the spanwise minimal domain (*S*180), the streamwise spectra near the channel centre contain a significant amount of energy at $\lambda_x^+ \simeq 400$–800, whereas its spanwise spectra at $\lambda_z^+ \leqslant 100$ have only little energy at the same wall-normal location. This implies that this part of the streamwise spectra is associated with essentially two-dimensional structures in the x–y plane resolved by $k_z = 0$. It is interesting to note that the streamwise length scale and the wall-normal location of the two-dimensional structures are reminiscent of Tollmien–Schlichting waves, which are supposed to be marginally stable at this Reynolds number: the Tollmien–Schlichting wave is composed of the intense wall-normal velocity with its peak location at the channel centre and with its streamwise wavelength $\lambda_x \simeq 6h$ (see e.g. Schmid & Henningson 2001). However, understanding such two-dimensional structures is beyond the scope of the present paper, and thus we avoid discussing it. Now, we apply the filtering (2.2) to the simulation with the spanwise minimal domain (*N*180). The streamwise spectra of the filtered case do not show the intense energy at the channel centre any more, suggesting that the filtering effectively removes the two-dimensional structures. Importantly, in the spanwise spectra, there is only little difference between *S*180 and *N*180, suggesting that the filtering (2.2) does not significantly distort the turbulent motions at $\lambda_z^+ \leqslant 100$.

3. Results

3.1. *Mean velocity profile and velocity fluctuations*

Mean velocity profiles and velocity fluctuations of the simulations, in which turbulent motions wider than $\lambda_z^+ \simeq 100$ are removed using the spanwise minimal domain and the filtering (2.2) (hereafter, we refer to this type of simulation as 'filtered simulation'), are presented in figure 3 up to $Re_\tau = 660$ (*N*180, *N*410 and *N*660). For comparison, DNS data by Abe, Kawamura & Choi (2004), which provide a Reynolds number ($Re_\tau = 640$) closest to the largest one of the filtered simulation, are drawn together. The mean velocity profiles from all the filtered simulations show good agreement with the full simulation below $y^+ \simeq 40$, although the data from *N*180 seem to deviate a little more than the others (figure 3*a*). However, as we discussed earlier, the mean velocity profile at $y^+ \leqslant 40$ from *N*180 also agrees very well with that of the full simulation at the same Reynolds number (figure 1*a*), suggesting that this deviation of *N*180 is likely to be due to the effect of the low Reynolds number.

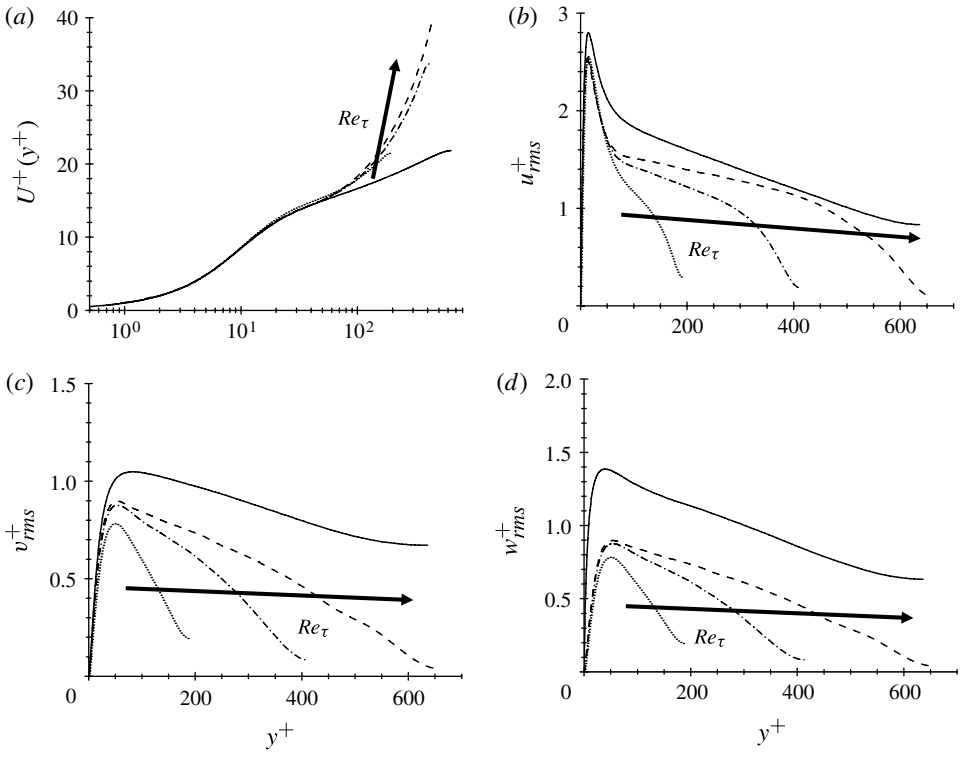

FIGURE 3. (*a*) Mean velocity profile $U^+(y^+)$ and turbulent velocity fluctuations (*b*) $u^+_{rms}(y^+)$, (*c*) $v^+_{rms}(y^+)$ and (*d*) $w^+_{rms}(y^+)$. Curves: ——, DNS by Abe *et al.* (2004) at $Re_\tau = 640$; · · · · · ·, $N180$; — · — · —, $N410$; - - - -, $N660$.

The velocity fluctuations are presented in figure 3(*b–d*). Comparison of the velocity fluctuations of the filtered simulation at $Re_\tau = 660$ ($N660$) with those of the full simulation at $Re_\tau = 640$ suggests that those of $N660$ are much smaller than those of the full simulation over the entire wall-normal domain. In particular, significant amounts of the spanwise velocity fluctuation are reduced even in the near-wall region, implying that the removal of the wider motions strongly affects the spanwise velocity fluctuations (figure 3*d*). Below $y^+ \simeq 40$, the streamwise velocity fluctuations from all the filtered simulations at the three different Reynolds numbers show very good agreement with each other (figure 3*b*): the near-wall maximum of all the cases is found at $y^+ \simeq 15$ with the value $u^+ \simeq 2.5$. However, in this region, the wall-normal and spanwise velocity fluctuations behave a little differently from the streamwise velocity fluctuation: their scaling with the inner units in the near-wall region does not look as good as that of the streamwise velocity fluctuation (figure 3*c*,*d*). In particular, their near-wall peaks at $Re_\tau \simeq 180$ are much smaller than those at $Re_\tau \simeq 410$ and 660. However, the only small difference between the near-wall peaks from $N410$ and $N660$ suggests that they may scale in the inner units for sufficiently large Reynolds numbers. Above $y^+ \simeq 40$, all the velocity fluctuations do not scale well in the inner units. Instead, they are non-negligibly large in this region, even though their values at the channel centre approach zero with the Reynolds number. However, as we shall see later in one-dimensional spectra (figure 5), the length scales associated with the fluctuations above $y^+ \simeq 40$ scale very well in the inner units, implying that they are

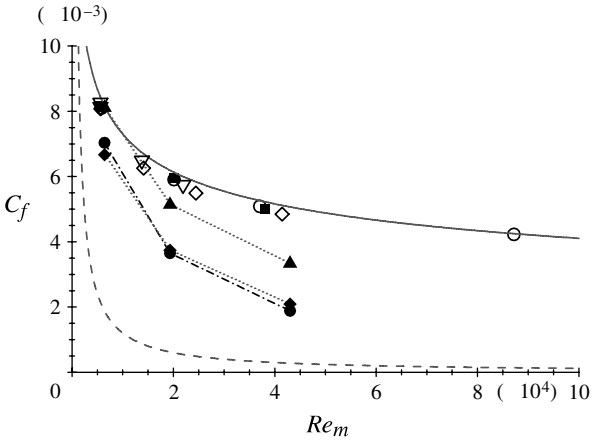

FIGURE 4. Variation of skin-friction coefficient with Re_m: ——, turbulent skin friction suggested by Dean (1978), $C_f = 0.073Re_m^{-0.25}$; - - - -, laminar skin friction, $C_f = 12/Re_m$; ▽, Kim *et al.* (1987) and Moser *et al.* (1999); ◯, del Álamo *et al.* (2004) and Hoyas & Jiménez (2006); ◇, Abe *et al.* (2004); ■, Hwang & Cossu (2010*c*) (LES), Hwang & Cossu (2011) (LES) and the present study (DNS); ●, the filtered simulations with $L_z^+ \simeq 100$ in the present study (*N*180, *N*410, *N*660); ◆, the simulations only with the spanwise minimal domain (*S*180, *S*410, *S*660); ▲, the filtered simulations with $L_z^+ \simeq 200$ (*L*180, *L*410, *L*660).

probably induced by interaction of the motions below $y^+ \simeq 40$ with the outer region supposed to be 'empty'.

Many features in the mean velocity profile and the velocity fluctuations are qualitatively similar to those observed in the early numerical experiment by Jiménez & Pinelli (1999), where the outer motions above a given wall-normal location ($y^+ \simeq 60$) are artificially damped out. For example, the mean velocity profile in the present study is also close to that of the laminar flow, and the shape of the near-wall velocity fluctuation is qualitatively similar to that of the full simulation. However, filtering wider than $\lambda_z^+ \simeq 100$ in the present study provides a better 'quantitative' scaling of the statistics in the inner units, which has not been obtained in the previous work.

3.2. *Skin-friction drag*

In figure 4, we report skin-friction coefficients from the filtered simulations with those from an empirical law of turbulent skin friction (Dean 1978), laminar skin friction and previous DNSs (Kim *et al.* 1987; Moser, Kim & Mansour 1999; Abe *et al.* 2004; del Álamo *et al.* 2004; Hoyas & Jiménez 2006). Direct simulation of the present study (*F*180) and large-eddy simulations of our previous studies (Hwang & Cossu 2010*c*, 2011) are also plotted to show the consistency of our code. The skin-friction coefficients from all the simulations with sufficiently large computational boxes (Kim *et al.* 1987; Moser *et al.* 1999; Abe *et al.* 2004; del Álamo *et al.* 2004; Hoyas & Jiménez 2006; Hwang & Cossu 2010*c*, 2011) show good agreement with the empirical law suggested by Dean (1978). However, the filtered simulations (*N*180, *N*410, *N*660) reveal smaller skin friction than these data at all the Reynolds numbers. Importantly, the difference between the skin frictions generated by the filtered and full simulations increases with the Reynolds number Re_m (● in figure 4). It should be emphasized that this small turbulent drag of the filtered simulations is not because the filtering (2.2) damages the nonlinear interaction related to $k_z = 0$; for example, the simulations

only with the spanwise minimal domain (*S*180, *S*410, *S*660) also show almost the same amounts of skin-friction reduction with the filtered simulations (♦ in figure 4). Therefore, this suggests that the removed motions (which are wider than $\lambda_z^+ \simeq 100$) are involved in substantial amounts of turbulent skin-friction generation and that their role becomes increasingly important with the increase of the Reynolds number.

With only the present results, it is not clear how the motions removed in the filtered simulations are exactly involved in generating turbulent skin friction particularly at high Reynolds numbers. It could be associated with lack of interaction of the near-wall motions with the outer ones such as large-scale and very-large-scale motions (Hutchins & Marusic 2007; Mathis *et al.* 2009). However, it seems that the motions in the logarithmic layer play an important role. To check this idea, we perform more simulations in which turbulent motions wider than $\lambda_z^+ \simeq 200$ are filtered out (*L*180, *L*410, *L*660; ▲ in figure 4). At the lowest Reynolds number, the *L*180 simulations are exposed to some motions in the wake outer region, as the largest spanwise length scale in this case is about $\lambda_z^+ \simeq 200$–400. Therefore, the skin friction in *L*180 does not show any substantial difference from that in the full simulation. However, at higher Reynolds numbers (*L*410 and *L*660), these simulations do not allow enough spanwise space for large-scale and very-large-scale motions. Nevertheless, the skin frictions by all these simulations are much increased compared to that in the simulation that filters out motions wider than $\lambda_z^+ \simeq 100$ (*N*180, *N*410, *N*660). More interestingly, the skin friction of these simulations also exhibits gradually increasing difference from that of full simulations, similarly to that of the simulations without motions wider than $L_z^+ \simeq 100$ (*N*180, *N*410, *N*660). This suggests that the gradual increase of the difference between the skin friction of the filtered and full simulations may originate from the increase of the filtered motions with the Reynolds number, many of which may populate the logarithmic layer.

3.3. *One-dimensional spectra*

The one-dimensional spectra of the filtered simulations at two different Reynolds numbers (*N*180 and *N*660) are shown in figure 5. Here, the one-dimensional spectra of each case are accumulated with slightly different L_z^+ (see table 1), and this is found to yield a small difference between the streamwise spectra of the two filtered simulations. For more accurate comparison, we therefore slightly corrected the streamwise wavelengths in each spectrum based on a relationship between the spanwise and streamwise wavelengths in the near-wall two-dimensional spectra. The detailed procedure for this correction is given in the Appendix.

The spanwise spectra of the streamwise velocity from both *N*180 and *N*660 have their maximum at $y^+ \simeq 10$–20 and $\lambda_z^+ \simeq 100$ (figure 5*a*). At this wall-normal location, the streamwise spectra show the largest value at $\lambda_x^+ \simeq 600$ (figure 5*b*). These spanwise and streamwise length scales correspond well to those of the near-wall streaks, although the streamwise one is a little shorter than the one often quoted ($\lambda_x^+ \simeq 1000$). As the wall-normal location moves further from the wall ($y^+ \geqslant 30$), both *N*180 and *N*660 reveal large energy at a shorter streamwise length scale, $\lambda_x^+ \simeq 300$, and this part of the spectra becomes more prominent with the increase of the Reynolds number.

In the spanwise and streamwise spectra of the wall-normal velocity, each maximum is respectively found at $\lambda_z^+ \simeq 100$ and $\lambda_x^+ \simeq 200$ for $y^+ \simeq 40$–50 (figure 5*c*,*d*). In contrast to the two different peaks that depend on the wall-normal location in the streamwise spectra of the streamwise velocity, the streamwise spectra of the wall-normal velocity reveal a single peak at $\lambda_x^+ \simeq 200$ over the entire wall-normal domain. Similar features are found for the spanwise velocity except in the region very close to

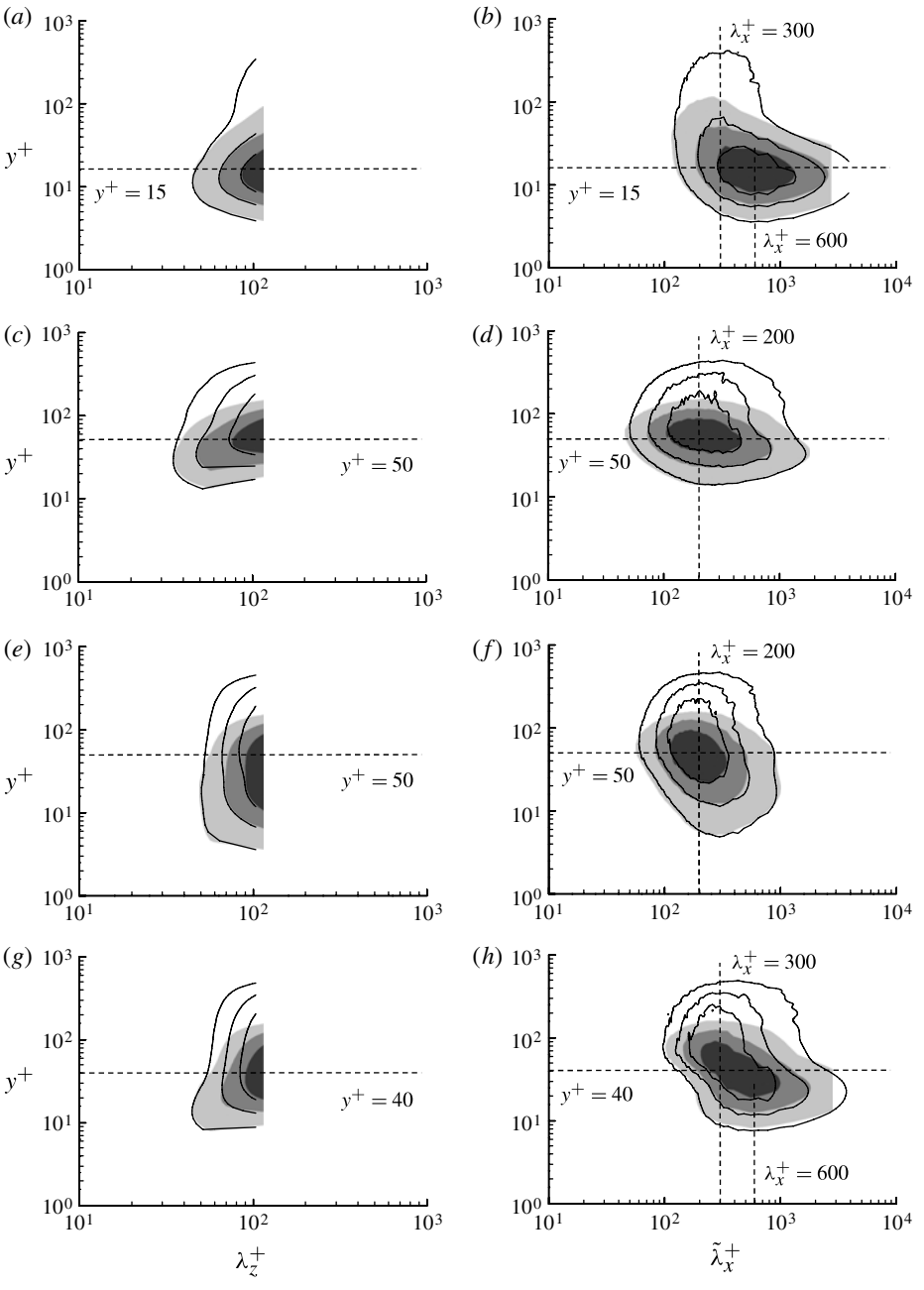

FIGURE 5. Premultiplied one-dimensional (*a*,*c*,*e*,*g*) spanwise and (*b*,*d*,*f*,*h*) streamwise spectra of (*a*,*b*) streamwise velocity, (*c*,*d*) wall-normal velocity, (*e*,*f*) spanwise velocity and (*g*,*h*) Reynolds stress. Here: shaded, *N*180; solid, *N*660. The contour labels are uniformly spaced from zero for comparison. For an accurate comparison of the spectra from the slightly different L_z^+ of *N*180 and *N*660, the streamwise wavelengths in each of the streamwise spectra are corrected such that $\tilde{\lambda}_x^+ = \lambda_x^+ \times (100/L_z^+)^2$ following the observation in the Appendix.

the wall: the spanwise velocity tends to penetrate deeper into the near-wall region than the wall-normal velocity (figure 5*e*,*f*) because the wall-normal velocity satisfies the impermeability condition ($\partial v/\partial y|_{y=0} = 0$). In the very near-wall region ($y^+ < 10$), the spanwise velocity fluctuation is slightly longer than that above this region (figure 5*f*). This is probably due to the effect of the long streamwise velocity fluctuations in this region because continuity requires at least some spanwise velocity fluctuations.

The streamwise length scale of the maxima in the spectra of the wall-normal and spanwise velocities ($\lambda_x^+ \simeq 200$–300) well depicts the streamwise extent of the near-wall streamwise vortices (Kim *et al.* 1987; Jeong *et al.* 1997). In the filtered simulations, these relatively short and tall motions are seen to be highly correlated with the streamwise velocity fluctuations above $y^+ \simeq 40$ (figure 5*a*,*b*), resulting in large Reynolds stress in this region (figure 5*g*,*h*). High correlation between the streamwise and wall-normal velocities is also observed below $y^+ \simeq 40$, but only at long streamwise length scales ($\lambda_x^+ \simeq 500$–600). This feature is consistent with the previous observation, where large Reynolds stress was found at long streamwise wavelengths (Jiménez *et al.* 2004).

In general, both the spanwise and streamwise spectra from the two filtered simulations *N*180 and *N*660 are in excellent agreement in the near-wall region ($y^+ \leqslant 40$). This suggests that the near-wall region of the filtered simulations scale very well in the inner units, and explains why the near-wall peaks of the streamwise velocity in the filtered simulations remain almost constant with the increase of the Reynolds number (figure 3*b*–*d*). Furthermore, as we have mentioned earlier, the very good scaling in the inner units implies that the spanwise filtering indeed effectively removes the log-layer and wake-outer-region motions affected in the near-wall region.

The one-dimensional spectra of the filtered simulation at $Re_\tau = 660$ (*N*660) are also compared with those of full simulation at $Re_\tau = 550$ (del Álamo *et al.* 2004) in figure 6. For all the variables considered here, the spanwise spectra of the filtered simulation show reasonable agreement with those of the full simulation below $y^+ \simeq 40$. However, above $y^+ \simeq 40$, turbulent fluctuations near $\lambda_z^+ \simeq 100$ of the filtered simulation carry much larger energy than those of the full simulation (figure 6*a*,*c*,*e*,*g*). The streamwise spectra of the filtered simulations indicate that the large energy at $\lambda_z^+ \leqslant 100$ is from the spectral peak of $\lambda_x^+ \simeq 300$ above $y^+ \simeq 40$ (figure 6*b*,*d*,*f*,*h*). This implies that the fluctuations above $y^+ \simeq 40$ in the filtered simulations are an artifact caused by the lack of motions wider than $\lambda_z^+ \simeq 100$ in the outer region.

Excluding the artifact of the filtered simulation above $y^+ \simeq 40$, the streamwise spectra of the filtered simulation clearly reveal significant amounts of lack of energy in the outer region for most of the streamwise wavelengths (figure 6*b*,*d*,*f*,*h*). Below $y^+ \simeq 40$, the streamwise and spanwise velocity spectra of the filtered simulation are respectively in reasonable agreement with those of the full simulation for $\lambda_x^+ \leqslant 600$ and $\lambda_x^+ \leqslant 200$ (figure 6*b*,*d*), indicating that they contain much less energy than those of the full simulation at long streamwise wavelengths in this region. In contrast, the wall-normal velocity fluctuations behave a little differently: the difference between the filtered and full simulations below $y^+ \leqslant 40$ is not as large as that of the streamwise and spanwise velocities (figure 6*d*). This kind of behaviour is also seen in the spectra of the Reynolds stress for $y^+ \leqslant 10$: there is no significant difference between the filtered and full simulations in the spectra of the very near-wall region ($y^+ \leqslant 10$), but in the region of $y^+ \geqslant 10$, the filtered simulation shows much less Reynolds stress for relatively long streamwise wavelengths.

Many features in the spectra discussed here are qualitatively similar to those in the early numerical experiment by Jiménez *et al.* (2004): for example, the spectra

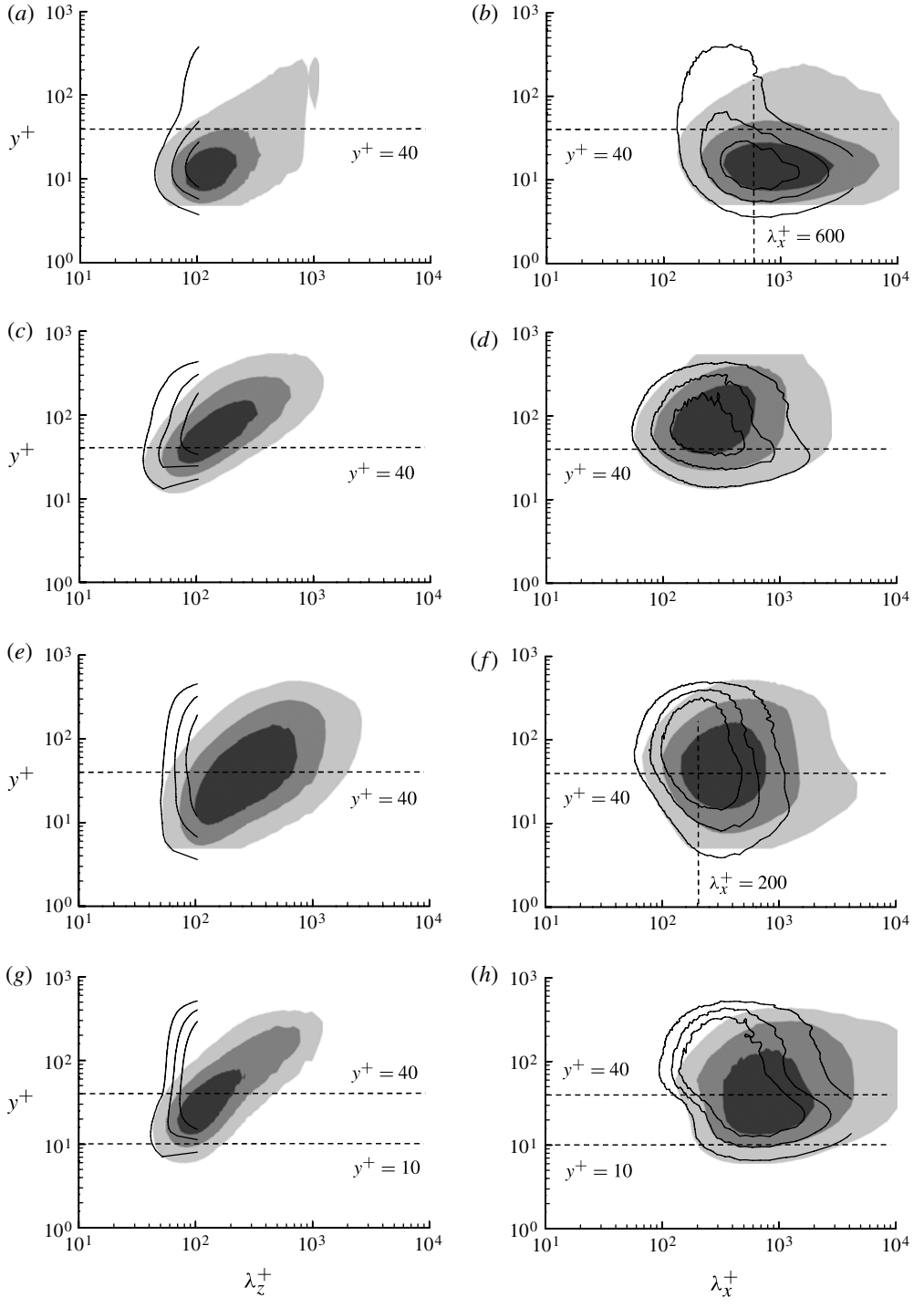

FIGURE 6. Premultiplied one-dimensional (*a*,*c*,*e*,*g*) spanwise and (*b*,*d*,*f*,*h*) streamwise spectra of (*a*,*b*) streamwise velocity, (*c*,*d*) wall-normal velocity, (*e*,*f*) spanwise velocity and (*g*,*h*) Reynolds stress. Here: shaded, from del Álamo *et al.* (2004); solid, *N*660. The contours labels are uniformly spaced from zero for comparison.

of the near-wall region are not significantly distorted in the absence of outer flows. The present numerical experiment confirms this early result, and shows that the method of removing the outer motions does not significantly affect the near-wall dynamics. Furthermore, we show that the near-wall spectra exhibit quantitatively good scaling only in the inner units for all the Reynolds numbers considered. However, an important difference is also seen particularly in the spectra of the streamwise velocity. In the numerical experiment by Jiménez *et al.* (2004), the streamwise spectra of the streamwise velocity reveal elongation: more intense energy is observed at long streamwise wavelength in the absence of the outer motions. However, this is not observed in the present numerical experiment. In fact, Jiménez *et al.* (2004) discussed that the streamwise elongation of the streamwise velocity spectra is due to the self-organization of each near-wall streak. We note that this self-organization is inhibited in the present study due to its narrow spanwise domain, and this explains why the streamwise spectra of the streamwise velocity in the present numerical experiments are shorter than those in Jiménez *et al.* (2004).

3.4. *Instantaneous flow field*

Instantaneous flow fields of the filtered simulations at two different Reynolds numbers ($N180$ and $N660$) are shown in figure 7, where iso-surfaces of the streamwise velocity fluctuation (u^+, dark grey/blue online) and the second invariant of the velocity-gradient tensor ($\boldsymbol{Q}$, light grey/yellow online) are drawn together. In both cases, the near-wall region is characterized by long streaky structures of the streamwise velocity fluctuation, and relatively short streamwise vortical structures are aligned with them, consistent with previous studies (Kline *et al.* 1967; Smith & Metzler 1983; Kim *et al.* 1987; Jeong *et al.* 1997; Jiménez *et al.* 2004). However, the flow field at $Re_\tau = 660$ reveals considerable amounts of the streamwise velocity and vortical structures above $y^+ \simeq 100$ as discussed with the one-dimensional spectra (figure 7*b*). The streamwise length scale of these structures is much shorter than that of the near-wall streaks, but is comparable to that of the near-wall streamwise vortical structures, consistent with the one-dimensional spectra. The vortical structures in this region also seem to be aligned along the streamwise direction, and it is difficult to identify arc-like vortices (Adrian 2007) at least in instantaneous flow fields.

4. Discussions

Thus far, we have presented results of the numerical experiment that artificially removes turbulent motions wider than $\lambda_z^+ \simeq 100$. As expected, these motions sustain by themselves and recover important features of the near-wall region observed in previous laboratory experiments and DNSs. The self-sustaining near-wall motions are also found to scale very well in the inner units only. The one-dimensional spectra and the flow field visualizations of the filtered simulations suggest that turbulent fluctuations narrower than $\lambda_z^+ \simeq 100$ mainly consist of two dominant motions: one is long ($\lambda_x^+ \simeq 600$) and highly confined to the near-wall region ($y^+ \leqslant 40$), and the other is relatively short ($\lambda_x^+ \simeq 200$–300) and quite tall in the absence of motions wider than $\lambda_z^+ \simeq 100$. The former is a dominant carrier of the near-wall streamwise velocity fluctuation, whereas the latter is composed of groups of individual vortical structures containing all the velocity components (see also figure 7*b*). The 'tall' characteristics of the latter thus refer to the wall-normal extent of the groups of vortical structures, and, in particular, the spanwise component of the grouped vortical structures penetrates deep into the near-wall region (figure 5*f*). The former very well describes the near-

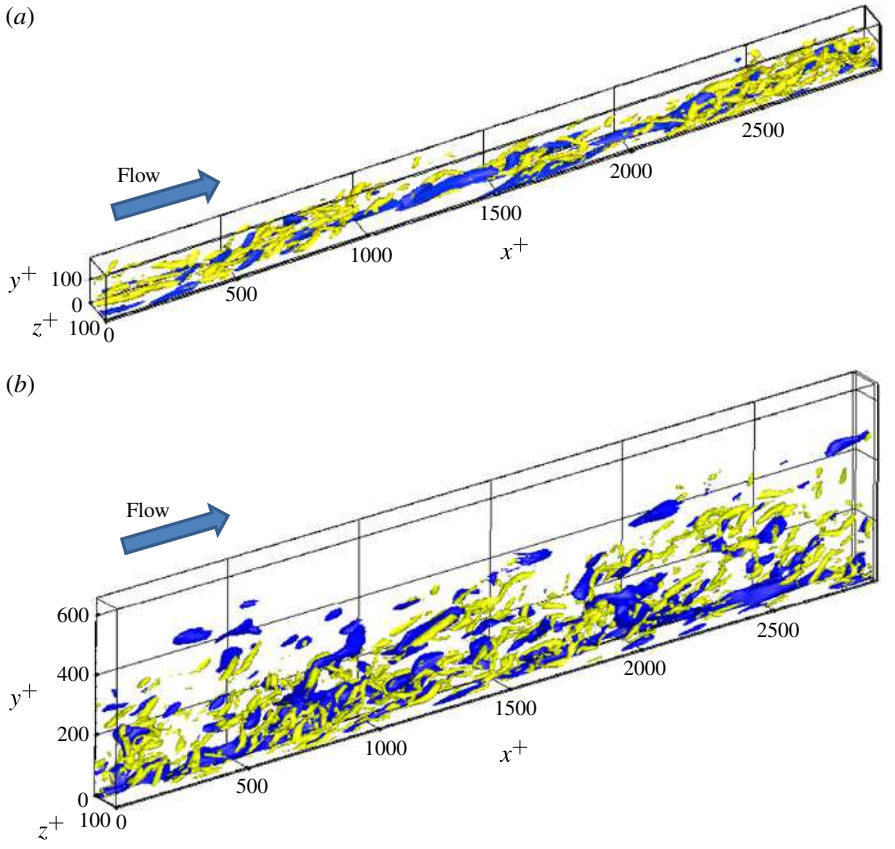

FIGURE 7. (Colour online) Instantaneous streamwise velocity fluctuations (dark grey/blue online) and vortical structures (light grey/yellow online) of (*a*) *N*180 ($u^+ = -2.5$, $\boldsymbol{Q}^+ = 0.0089$) and (*b*) *N*660 ($u^+ = -2.5$, $\boldsymbol{Q}^+ = 0.016$).

wall streaks (Kline *et al.* 1967; Smith & Metzler 1983; Kim *et al.* 1987) and the latter depicts well the quasi-streamwise vortices (Kim *et al.* 1987; Jeong *et al.* 1997), at least in the near-wall region ($y^+ \simeq 40$).

In the filtered simulations, the motions associated with the quasi-streamwise vortices carry significant turbulent fluctuations in the outer region, which is supposed to be 'empty' in the absence of wide log-layer and wake-outer-region motions. They are found to be non-negligible even around the channel centre (figure 3*b–d*). However, it should be mentioned that the tall part of the motions is not likely to be the direct outcome of the outer flow itself because the length of the tall fluctuation still scales very well in the inner units ($\lambda_z^+ \simeq 100$ and $\lambda_x^+ \simeq 200$–300). It is interesting to note that the minimal box experiment by Jiménez & Pinelli (1999) provides an interesting scaling argument in this regard: they suggest that restricting the spanwise length scale may produce non-decaying vortical fluctuations in the wall-normal direction (for further details, see Jiménez & Pinelli 1999). We also note that the tall part is not essential for the survival of the near-wall turbulence, as seen in the filtered simulation at low Reynolds number (*N*180), where the fluctuation above $y^+ \simeq 180$ is completely inhibited by a geometric constraint (height of the channel). This is also consistent with previous numerical experiments where turbulent fluctuations above a certain wall-

normal location are artificially damped out (Jiménez & Pinelli 1999; Jiménez *et al.* 2004). Finally, it should be pointed out that the appearance of the tall motions may be partially contributed by the method of filtering out the wide outer motions, as the real outer motions interact with a range of scales near the cut-off spanwise wavelength $\lambda_z^+ \simeq 100$ (Saikrishnan *et al.* 2012). Therefore, the statistical structures of the tall motions may not be entirely physical and they may also depend on the choice of the filter.

4.1. *Near-wall streaks and formation of mean velocity profiles*

The mean velocity profiles of the filtered simulations at all the Reynolds numbers considered here reveal that they are in good agreement with those of full simulations below $y^+ \simeq 40$. The wall-normal location, below which the mean velocity agrees well with full simulations, is consistent with scaling $y^+ \sim 0.3L_z^+$, recently proposed by Flores & Jiménez (2010). It should be pointed out that the streamwise velocity fluctuation in this region is dominantly characterized by the near-wall streaks (figure 5*b*). It is interesting to compare this behaviour with a recent study where the mean behaviour of fully developed turbulent plane Couette flow is well recovered by a streamwise constant projection of the stochastically driven nonlinear Navier–Stokes equation (Gayme *et al.* 2010). The stochastically driven wall flows have been shown to easily amplify the long streaky motions (Jovanović & Bamieh 2005; Hwang & Cossu 2010*a*,*b*; Willis *et al.* 2010; Gayme *et al.* 2011). Thus it is likely that the flow field in that study is mainly characterized by the streamwise uniform streaks. This finding is very similar to the behaviour of the mean velocity profile below $y^+ \simeq 40$ in the present study, suggesting that the long near-wall streaks, amplified large enough to be influenced by nonlinearity, play a crucial role in the formation of the proper mean velocity profile in the near-wall region.

4.2. *Turbulent skin friction and the outer structures*

One of the most interesting findings in the present study may be the contribution of the self-sustaining near-wall motions to turbulent skin friction. At the lowest Reynolds number considered in the present study ($N180$), turbulent skin friction of the filtered simulation is found to be only a little smaller than that of the full simulation. However, the skin friction at the highest Reynolds number ($N660$) is considerably smaller than the turbulent skin friction generated by the full simulation (figure 4). Although the present simulations are still limited to relatively low Reynolds numbers, the trend of the data clearly suggests that the contribution of motions narrower than $\lambda_z^+ \simeq 100$ to the total turbulent skin friction decreases with the Reynolds number. This implies that turbulent skin friction directly associated with the self-sustaining near-wall motions might be very small at very high Reynolds numbers. However, this behaviour might have been expected. It has recently become evident that large amounts of outer turbulent fluctuations penetrate deep into the near-wall region (De Graaff & Eaton 2000; del Álamo & Jiménez 2003; Hutchins & Marusic 2007) and that they even modulate the near-wall processes (Mathis *et al.* 2009). This inner–outer interaction has also been quantitatively assessed with interesting models that predict the near-wall behaviour with information only on the outer motions (Marusic, Mathis & Hutchins 2010*a*; Mathis *et al.* 2013). However, it should be emphasized that dynamics in the logarithmic layer also plays a crucial role in turbulent skin-friction generation, as seen in the simulation results of $L180$, $L410$ and $L660$ in which motions wider than $\lambda_z^+ \simeq 200$ are removed (see ▲ in figure 4).

This finding in the present study suggests that turbulent skin friction is probably generated by motions at all the length scales, i.e. the inner ($N180$, $N410$, $N660$), log-layer ($L180$, $L410$, $L660$) and outer (DNS in previous studies) scales. At low Reynolds numbers, the near-wall motion plays a major role in the skin-friction generation due to the lack of length scale separation between the inner and outer units (compare skin frictions between $N180$ and $F180$ in figure 4). Although the result in this case might contain some influence of the outer flow, this behaviour is consistent with early investigations where the skin-friction generation at low Reynolds numbers is highly correlated to the near-wall motions (particularly the streamwise vortices) (Kravchenko, Choi & Moin 1993; Choi, Moin & Kim 1994; Orlandi & Jimenez 1994). As the Reynolds number increases, large numbers of log-layer structures, the size of which spans from the inner to the outer length scale, appear. The $L180$, $L410$ and $L660$ simulations suggest that these structures are indeed involved in turbulent skin-friction generation. However, the role of the outer structures such as large-scale and very-large-scale motions should also be taken into account, as they also penetrate deep into the near-wall region. It should be emphasized that this interpretation is consistent with the attached-eddy hypothesis (e.g. Townsend 1976), which also explains the logarithmic increase of the near-wall peak of the streamwise turbulence intensity (see also discussion in § 4.3).

A little evidence supporting the present observation also appears in the flow-control literature. For example, the opposition control, which is designed to directly suppress near-wall streamwise vortices using blowing and suction at the wall (Choi *et al.* 1994), shows the decrease of the maximum amount of turbulent drag reduction with the Reynolds number (Chang, Collis & Ramakrishnan 2002). Similar behaviour was also recently observed in controls using spanwise wall oscillations (e.g. Karniadiakis & Choi 2003): a few recent studies on this type of skin-friction control recently reported that the amount of turbulent skin-friction reduction gradually decays with the increase of the Reynolds number (Ricco & Quadrio 2008; Touber & Leschziner 2012). Interestingly, Touber & Leschziner (2012) addressed the idea that the decay of the amount of turbulent skin-friction reduction with the Reynolds number in this control approach is due to the influence of the large-scale outer structures. It is interesting to note that both the control approaches mentioned here are designed to disturb only near-wall processes: the opposition control attempts to directly weaken the near-wall streamwise vortices (Choi *et al.* 1994), and the spanwise wall oscillation disturbs the near-wall streamwise vortices with the Stokes layer formed by the wall oscillation (Karniadiakis & Choi 2003). Although more evidence needs to be accumulated, the undesirable performance decay of these control approaches with the Reynolds number might be because the contribution of the self-sustaining near-wall dynamics to turbulent skin friction itself decays with the Reynolds number.

Nevertheless, the small contribution of the near-wall motions to turbulent skin friction could be good news from the viewpoint of engineering application. Controlling the near-wall structures is known to be a very challenging issue because of their very small length scale. For example, the typical spanwise length scale of the near-wall motions ($\lambda_z^+ \leqslant 100$) observed in the operating range of commercial aircraft is $O(0.01\text{–}0.1$ mm) (Kasagi, Suzuki & Fukagata 2008), implying that micro-scale devices would be required if one aims to directly manipulate the near-wall motions. However, as shown in the present study, the contribution of structures wider than $\lambda_z^+ \simeq 100$ to turbulent skin friction would also be very important at high Reynolds numbers. Therefore, at sufficiently high Reynolds numbers, one might be successful in reducing turbulent skin friction by manipulating coherent motions larger than the near-wall

motions. However, to our best knowledge, no study has provided any evidence of turbulent skin-friction reduction only by suppressing the turbulent structures larger than the near-wall motions. Only a few recent studies have shown that forcing the large-scale outer motions with an appropriate amount of energy input results in turbulent skin-friction reduction (Schoppa & Hussain 1998; Willis *et al.* 2010), but, even in those studies, the forcing was used to modify the near-wall dynamics by manipulating the outer motions instead of suppressing them.

4.3. *The near-wall turbulent fluctuations and the attached-eddy scenario*

Recent investigations have found that the near-wall region of wall-bounded turbulent flows is largely influenced by the outer flows (del Álamo & Jiménez 2003; Hoyas & Jiménez 2006; Hutchins & Marusic 2007; Mathis *et al.* 2009). Consistent with these observations, the turbulent motions narrower than $\lambda_z^+ \simeq 100$ reveal significant amounts of lack of near-wall turbulent fluctuations at long streamwise length scales, which are probably associated with the removed log-layer and wake-outer-region motions. In particular, the streamwise and spanwise velocity fluctuations in the near-wall region of the filtered simulations are found to have much shorter streamwise length scales than those of the full simulations (figure 5*b*,*f*). In contrast, the loss of the energy of the wall-normal velocity and Reynolds stress at long streamwise length scales in the near-wall region is not so severe as that of the streamwise and spanwise velocities (figure 5*d*,*h*). This observation is consistent with a recent study by Jiménez & Hoyas (2008) where they classified the streamwise and spanwise velocities into 'attached (anchored)' variables and the wall-normal velocity and the Reynolds stress into 'detached (floating)' variables. In this study, the attached variables are defined to carry substantial energy near the wall, while the detached ones are defined not to. It should be mentioned that this kind of classification is essential to support the attached-eddy scenario (e.g. logarithmic wall-normal profiles of the streamwise and spanwise velocity fluctuations). Therefore, this implies that the results of the present numerical experiments also support the attached-eddy scenario above the near-wall region (Townsend 1976; Perry & Chong 1982; Perry *et al.* 1986).

The scaling of the near-wall peak in the streamwise velocity fluctuation with the Reynolds number has recently been an important issue. Recent investigations have convincingly shown that the near-wall streamwise velocity fluctuations increase, with a logarithmic dependence on the Reynolds number (De Graaff & Eaton 2000; Metzger & Klewicki 2001; Marusic & Kunkel 2003; Hoyas & Jiménez 2006). De Graaff & Eaton (2000) initially proposed a mixed scaling with $u_\tau U_\infty$ based on their measurement in a turbulent boundary layer (here, U_∞ is the free stream velocity). However, later interpretations have proposed that the increase of the streamwise velocity fluctuation is likely to be due to the collective contributions of the attached eddies to the near-wall region (Marusic & Kunkel 2003; Jiménez & Hoyas 2008). It is important to note that this also explains the mixed scaling by De Graaff & Eaton (2000) because $U_\infty \sim u_\tau \ln Re_\tau$.

In the present numerical experiment, we removed motions wider than $\lambda_z^+ \simeq 100$. The removed motions are probably include the log-layer and wake-outer-region motions. Therefore, to be consistent with the previous studies, the streamwise velocity fluctuations in the filtered simulations should scale well only in the inner units. Indeed, the removal of the motions wider than $\lambda_z^+ \simeq 100$ provides almost a constant value of the near-wall peak of the streamwise velocity fluctuation at all the Reynolds numbers considered. This result directly supports the previous interpretations where the increase

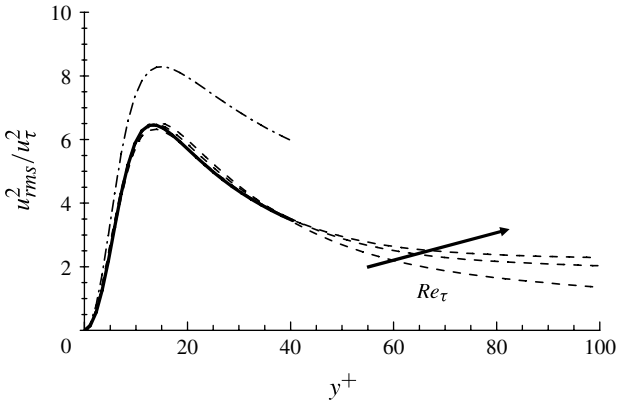

FIGURE 8. Streamwise turbulent kinetic energy profiles: - - - -, the filtered simulations ($N180$, $N410$ and $N660$); ——, $f_1(y^+)$ with the fitting constants in (4.2); — · — · —, $f_1(y^+)$ with the fitting constants in Marusic & Kunkel (2003).

of the near-wall peak of the streamwise velocity is due to the log-layer and wake-outer-region motions carrying substantial turbulence near the wall.

Finally, the results of the present numerical experiment can also be used to tune some empirical curves for prediction of turbulence intensity at high Reynolds numbers. Marusic & Kunkel (2003) proposed that the streamwise velocity fluctuation in the near-wall region would be described as the multiplication of two components based on the attached-eddy scenario: $u^2_{rms}/u^2_\tau = f_1(y^+) f_T(y^+, Re_\tau)$, where $f_1(y^+)$ is a universal function completely scaling in the inner units, and $f_T(y^+, Re_\tau)$ is a forcing function by the outer turbulence accounting for its logarithmic dependence with the Reynolds number. An empirical curve of $f_1(y^+)$ was proposed by that study as

$$f_1(y^+) = \frac{a_1 \, (y^+)^2}{\left(1 + a_2 \, (y^+)^2\right)^{1/2} \left(1 + (a_3 y^+)^{2a_4}\right)^{1/2}}, \tag{4.1}$$

where the fitting constants are given as $a_1 = 0.16$, $a_2 = 0.008$, $a_3 = 0.115$ and $a_4 = 1.6$. Here, these constants were originally tuned based on the measurement data of a turbulent boundary layer at $Re_\tau = 2000$ (De Graaff & Eaton 2000). Therefore, the proposed curve would not be strictly valid below $Re_\tau = 2000$, although this Reynolds number may not be high enough to be considered as the high-Reynolds-number regime. In the present study, the removal of structures wider than $\lambda_z^+ \simeq 100$ provides near-wall streamwise velocity fluctuations almost independent of the Reynolds number. Therefore, it would be more appropriate to tune the curve $f_1(y^+)$ based on our numerical experiment. Based on trial and error, the present numerical experiment enables us to propose new fitting constants as follows:

$$a_1 = 0.113, \quad a_2 = 0.008, \quad a_3 = 0.10, \quad a_4 = 1.9. \tag{4.2}$$

The empirical curve (4.1) with these fitting constants is shown in figure 8 with the data from the filtered simulations. The newly tuned fitting curve is in good agreement with the data from the present numerical experiment below $y^+ \simeq 40$. We note that the fitting curve with the constants (4.2) appears to be smaller than that in Marusic & Kunkel (2003) over the given wall-normal domain because their curve contains the outer-flow influence at $Re_\tau = 2000$.

5. Concluding remarks

In the present study, we carry out a numerical experiment that removes turbulent motions wider than $\lambda_z^+ \simeq 100$ up to $Re_\tau = 660$ ($Re_m = 43\,010$). The main findings of the present study are summarized as follows.

(*a*) The mean velocity profile of the self-sustaining motions narrower than $\lambda_z^+ \simeq 100$ shows very good agreement with that of full simulations below $y^+ \leqslant 40$. In this region, the streamwise velocity fluctuations of these motions scale very well in the inner units, and they remain almost constant at all the Reynolds numbers considered here. The spanwise and wall-normal velocity fluctuations seem to exhibit similar behaviour at least for $Re_\tau > 500$.

(*b*) The self-sustaining motions for $\lambda_z^+ \leqslant 100$ exhibit smaller turbulent skin friction than the entire turbulent motions. The difference between the turbulent skin frictions of the two motions gradually increases with the Reynolds number, indicating that the contribution of the self-sustaining motions narrower than $\lambda_z^+ \simeq 100$ to turbulent skin friction decays with the increase of the Reynolds number.

(*c*) The one-dimensional spectra of the motions for $\lambda_z^+ \leqslant 100$ scale very well in the inner units below $y^+ \simeq 40$. The spectra suggest that the turbulent fluctuations are composed of two modes: one is highly confined below $y^+ \leqslant 30$ with intense streamwise velocity fluctuations at $\lambda_x^+ \simeq 600$–700, and the other even reaches near to the channel centre at all the Reynolds numbers considered and carries fluctuations of all the velocity components with the streamwise length scale, $\lambda_x^+ \simeq 200$–300. Below $y^+ \simeq 40$, the former well describes the near-wall streaks and the latter well depicts the quasi-streamwise vortices.

(*d*) In the near-wall region, the streamwise and spanwise velocity fluctuations of the motions for $\lambda_z^+ \leqslant 100$ lack significant amounts of energy for large streamwise wavelengths compared to those of the full turbulent motions. This implies that these components of the motions wider than $\lambda_z^+ \simeq 100$ significantly contribute to the near-wall region. In contrast, the wall-normal velocity and the Reynolds stress of the the motions for $\lambda_z^+ \leqslant 100$ show relatively small amounts of energy loss at long streamwise length scales in the near-wall region. This finding is consistent with Jiménez & Hoyas (2008), and also supports the attached-eddy hypothesis (Townsend 1976; Perry & Chong 1982; Perry *et al.* 1986).

These findings are certainly consistent with the early studies where the near-wall turbulent motions were viewed as an outcome of processes independent of the outer turbulence (Jiménez & Moin 1991; Hamilton *et al.* 1995; Jiménez & Pinelli 1999; Schoppa & Hussain 2002; Jiménez *et al.* 2004). In particular, many important statistical features in the mean velocity, turbulence intensity and spectra found in the present study confirm the results in previous pioneering numerical experiments where the removal of outer turbulence does not change the essential features of the near-wall region (Jiménez & Pinelli 1999; Jiménez *et al.* 2004). The present study complements these early findings in the quantitative respect: removing the motions wider than $\lambda_z^+ \simeq 100$ shows that the statistics and spectra of the self-sustaining motions scale almost completely in the inner units at least in the near-wall region ($y^+ \leqslant 40$). This finding provides convincing evidence that the logarithmic growth of the near-wall streamwise turbulence intensity with the Reynolds number is at least not due to the near-wall self-sustaining motions themselves.

Probably, the most important finding in the present study is that the contribution of the near-wall self-sustaining motions to the skin friction is shown to decay with the

Reynolds number. This new observation suggests that motions wider than $\lambda_z^+ \simeq 100$, which includes the structures in both the logarithmic layer and the wake region, are strongly involved in the near-wall skin-friction generation at high Reynolds numbers. This feature might explain why some flow control strategies aimed only at the near-wall motions have not been very successful at high Reynolds numbers (Chang *et al.* 2002; Touber & Leschziner 2012). Importantly, it suggests that, at high Reynolds numbers, strategies targeting length scales relatively larger than the near-wall one would probably be required, and this remains an important work to be addressed in the near future from the viewpoint of engineering applications.

Another important goal for future study is to extend the present work to the spanwise length scales relevant to the logarithmic layer. Combining the over-damped LES (Hwang & Cossu 2010*c*) with the present approach would probably enable us to isolate the statistics of attached eddies of a given length scale, as recently shown by our preliminary work (Hwang & Cossu 2011). The follow-up work, aimed at computing the statistics of the attached eddies at a given length scale and comparing them with those hypothesized by Townsend (1976, see page 155), is currently under active investigation.

Acknowledgements

This paper was written just before I left the Laboratoire d'Hydrodynamique at École Polytechnique (LadHyX). I gratefully acknowledge Professors P. Huerre, C. Cossu, A. I. Barakat, J.-M. Chomaz, and people at LadHyX for their hospitality and generous support during my stay in the lab.

Appendix. Correction of streamwise spectra for comparison

Here, we present the correction of the streamwise wavelengths for the comparison of the streamwise spectra from slightly different L_z^+ of $N180$ and $N660$ (figure 5*b*,*d*,*f*,*h*). Figure 9(*a*) shows the premultiplied streamwise spectra of the streamwise velocity from $N180$, $N410$ and $N660$, and they are not very different from each other at $y^+ \simeq 40$. In particular, the agreement between data from $N410$ and $N660$ is fairly good. However, the difference between those from $N180$ and $N660$ is not negligible, and it is seen that the spectrum of $N180$ is a little shifted to the long-wavelength side. In fact, the spectrum of $N410$ is also slightly shifted to the long-wavelength side. It should be emphasized that this difference does not originate from the Reynolds number: the spanwise spectra of all the filtered simulations show very good agreement below $y^+ \simeq 40$, as shown in figure 5. We note that the larger the L_z^+ of the simulation is, the more the streamwise spectra are shifted to the long-wavelength side (see also table 1), suggesting that the difference in the spectra is probably the result of the slightly different L_z^+ of each filtered simulation.

For more accurate comparison, a correction of the streamwise wavelengths in the one-dimensional spectra is made based on two-dimensional spectra in the near-wall region. Figure 10 shows the two-dimensional spectra of the streamwise velocity at $y^+ \simeq 19$ from $N180$ and $F180$. The two-dimensional spectra of the filtered simulation show good agreement with those of the full simulation at this location. The two-dimensional spectra of the full simulation ($F180$) are found to be aligned along the curve $\lambda_x^+ \sim \lambda_z^{+3}$ as in previous studies (del Álamo & Jiménez 2003; Jiménez *et al.* 2004). However, in the range that the filtered simulations take into account (the rectangular box with thick solid line in figure 10), the two-dimensional spectra seem to be aligned along the curve $\lambda_x^+ \sim \lambda_z^{+2}$. This observation suggests that the

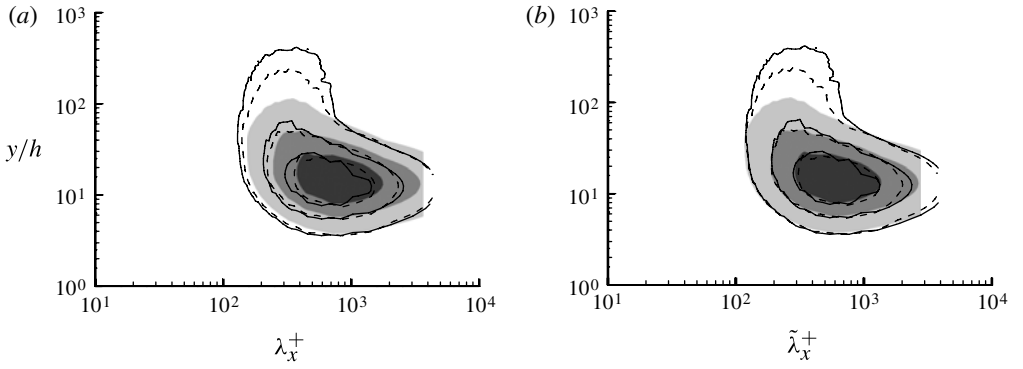

FIGURE 9. Premultiplied streamwise spectra of the streamwise velocity (*a*) before and (*b*) after the correction (A 1): shaded, *N*180; dashed, *N*410; solid, *N*660. The contour labels are chosen as 0.25, 0.5 and 0.75 times the maximum.

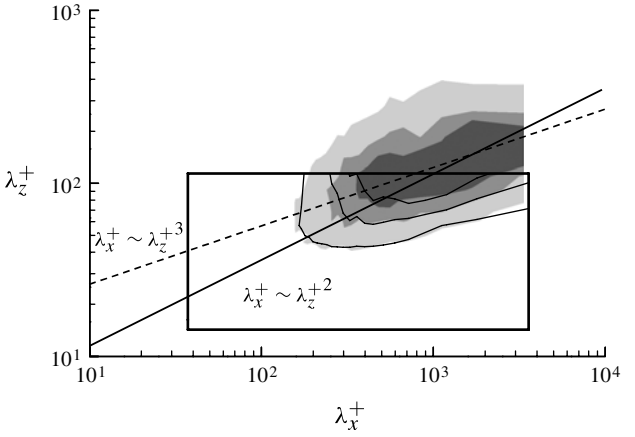

FIGURE 10. Two-dimensional spectra of the streamwise velocity, where the shaded and solid contours are, respectively, from *F*180 and *N*180. Here, the solid and dashed lines indicate $\lambda_x^+ \sim \lambda_z^{+2}$ and $\lambda_x^+ \sim \lambda_z^{+3}$, respectively.

amount of shift of the streamwise spectra to the long-wavelength side in the filtered simulations is probably proportional to L_z^{+2}. Therefore, the streamwise wavelength of the streamwise spectra of the filtered simulation is corrected so that

$$\tilde{\lambda}_x^+ = \lambda_x^+ \left(\frac{L_{z0}^+}{L_z^+} \right)^2. \tag{A 1}$$

Here, $L_{z0}^+ = 100$ is chosen from the given scope of the present study. The streamwise spectra of the streamwise velocity with the corrected wavelength $\tilde{\lambda}_x^+$ are presented in figure 9(*b*), and they show much better agreement than those before the correction (figure 9*a*).

REFERENCES

ABE, H., KAWAMURA, H. & CHOI, H. 2004 Very large-scale structures and their effects on the wall shear-stress fluctuations in a turbulent channel flow up to $Re = 640$. *J. Fluid Engng* **126**, 835–843.

ADRIAN, R. J. 2007 Hairpin vortex organization in wall turbulence. *Phys. Fluids* **19**, 041301.

DEL ÁLAMO, J. C. & JIMÉNEZ, J. 2003 Spectra of the very large anisotropic scales in turbulent channels. *Phys. Fluids* **15**, L41–L44.

DEL ÁLAMO, J. C. & JIMÉNEZ, J. 2006 Linear energy amplification in turbulent channels. *J. Fluid Mech.* **559**, 205–213.

DEL ÁLAMO, J. C., JIMÉNEZ, J., ZANDONADE, P. & MOSER, R. D. 2004 Scaling of the energy spectra of turbulent channels. *J. Fluid Mech.* **500**, 135–144.

DEL ÁLAMO, J. C., JIMÉNEZ, J., ZANDONADE, P. & MOSER, R. D. 2006 Self-similar vortex clusters in the turbulent logarithmic region. *J. Fluid Mech.* **561**, 329–358.

BUTLER, K. M. & FARRELL, B. F. 1993 Optimal perturbations and streak spacing in wall-bounded turbulent shear flow. *Phys. Fluids* **5**, 774–777.

CHANG, Y., COLLIS, S. S. & RAMAKRISHNAN, S. 2002 Viscous effects in control of near-wall turbulence. *Phys. Fluids* **14** (11), 4069–4080.

CHOI, H., MOIN, P. & KIM, J. 1994 Active turbulence control for drag reduction in wall-bounded flows. *J. Fluid Mech.* **262**, 75–110.

COSSU, C., PUJALS, G. & DEPARDON, S. 2009 Optimal transient growth and very large-scale structures in turbulent boundary layers. *J. Fluid Mech.* **619**, 79–94.

DE GRAAFF, D. B. & EATON, J. K. 2000 Reynolds-number scaling of the flat-plate turbulent boundary layer. *J. Fluid Mech.* **422**, 319–346.

DEAN, R. B. 1978 Reynolds number dependence of skin friction and other bulk flow variables in two-dimensional rectangular duct flow. *Trans. ASME: J. Fluids Engng* **100**, 215–233.

FAISST, H. & ECKHARDT, B. 2003 Travelling waves in pipe flow. *Phys. Rev. Lett.* **91**, 224502.

FLORES, O. & JIMÉNEZ, J 2010 Hierarchy of minimal flow units in the logarithmic layer. *Phys. Fluids* **22**, 071704.

GANAPATHISUBRAMANI, B., HUTCHINS, N., HAMBLETON, W. T., LONGMIRE, E. K. & MARUSIC, I. 2005 Investigation of large-scale coherence in a turbulent boundary layer using two-point correlation. *J. Fluid Mech.* **524**, 57–80.

GAYME, D. F., MCKEON, B. J., BAMIEH, B., PAPACHRISTODOULOU, A. & DOYLE, J. C. 2011 Amplification and nonlinear mechanisms in plane Couette flow. *Phys. Fluids* **23**, 065108.

GAYME, D. F., MCKEON, B. J., PAPACHRISTODOULOU, A., BAMIEH, B. & DOYLE, J. C. 2010 A streamwise constant model of turbulence in plane Couette flow. *J. Fluid Mech.* **665**, 99–119.

GIBSON, J. F., HALCROW, J. & CVITANOVIC, P. 2008 Visualizing the geometry of state space in plane Couette flow. *J. Fluid Mech.* **611**, 107–130.

HAMILTON, J. M., KIM, J. & WALEFFE, F. 1995 Regeneration mechanisms of near-wall turbulence structures. *J. Fluid Mech* **287**, 317–348.

HOYAS, S. & JIMÉNEZ, J. 2006 Scaling of the velocity fluctuations in turbulent channels up to $Re_\tau = 2003$. *Phys. Fluids* **18**, 011702.

HUTCHINS, N. & MARUSIC, I. 2007 Evidence of very long meandering features in the logarithmic region of turbulent boundary layers. *J. Fluid Mech.* **579**, 1–28.

HWANG, Y. & COSSU, C. 2010*a* Amplification of coherent streaks in the turbulent Couette flow: an input–output analysis at low Reynolds number. *J. Fluid Mech.* **643**, 333–348.

HWANG, Y. & COSSU, C. 2010*b* Linear non-normal energy amplification of harmonic and stochastic forcing in the turbulent channel flow. *J. Fluid Mech.* **664**, 51–73.

HWANG, Y. & COSSU, C. 2010*c* Self-sustained process at large scales in turbulent channel flow. *Phys. Rev. Lett.* **105**, 044505.

HWANG, Y. & COSSU, C. 2011 Self-sustained processes in the logarithmic layer of turbulent channel flows. *Phys. Fluid* **23**, 061702.

JEONG, J., BENNEY, F., SCHOPPA, W. & KIM, J. 1997 Coherent structures near the wall in a turbulent channel flow. *J. Fluid Mech.* **332**, 185–214.

JIMÉNEZ, J., DEL ÁLAMO, J. C. & FLORES, O. 2004 The large-scale dynamics of near-wall turbulence. *J. Fluid Mech.* **505**, 179–199.

JIMÉNEZ, J. & HOYAS, S. 2008 Turbulent fluctuations above the buffer layer of wall-bounded flows. *J. Fluid Mech.* **611**, 215–236.

JIMÉNEZ, J., KAWAHARA, G., SIMENS, M. P., NAGATA, M. & SHIBA, M. 2005 *Phys. Fluids* **17**, 015105.

JIMÉNEZ, J. & MOIN, P. 1991 The minimal flow unit in near-wall turbulence. *J. Fluid Mech.* **225**, 213–240.

JIMÉNEZ, J. & PINELLI, A. 1999 The autonomous cycle of near-wall turbulence. *J. Fluid Mech.* **389**, 335–359.

JOVANOVIĆ, M. R. & BAMIEH, B. 2005 Componentwise energy amplification in channel flow. *J. Fluid Mech.* **543**, 145–183.

KARNIADIAKIS, G. E. & CHOI, K. S. 2003 Mechanisms on transverse motions in turbulent wall flows. *Annu. Rev. Fluid Mech.* **35**, 45–62.

KASAGI, N., SUZUKI, Y. & FUKAGATA, K. 2008 Microelectromechanical systems based feedback control of turbulence for skin friction reduction. *Annu. Rev. Fluid Mech.* **41**, 231–251.

KIM, J. & MOIN, P 1985 Application of a fractional-step method to incompressible Navier–Stokes equations. *J. Comput. Phys.* **59**, 308–323.

KIM, J., MOIN, P. & MOSER, R. D. 1987 Turbulence statistics in fully developed channel flow at low Reynolds number. *J. Fluid Mech.* **177**, 133–166.

KLINE, S. J., REYNOLDS, W. C., SCHRAUB, F. A. & RUNSTADLER, P. W. 1967 The structure of turbulent boundary layers. *J. Fluid Mech.* **30**, 741–773.

KRAVCHENKO, A. G., CHOI, H. & MOIN, P. 1993 On the relation of near-wall streamwise vortices to wall skin friction in turbulent boundary layers. *Phys. Fluids* A **5**, 3307–3309.

LANDAHL, M. T. 1990 On sublayer streaks. *J. Fluid Mech.* **212**, 593–614.

MARUSIC, I. & KUNKEL, G. J. 2003 Streamwise turbulent intensity formulation for flat-plate boundary layers. *Phys. Fluids* **15** (8), 2461–2464.

MARUSIC, I., MATHIS, R. & HUTCHINS, N. 2010*a* Predictive model for wall-bounded turbulent flow. *Science* **329**, 193–196.

MARUSIC, I., MCKEON, B. J., MONKEWITZ, P. A., NAGIB, H. M., SMITS, A. J. & SREENIVASAN, K. R. 2010*b* Wall-bounded turbulent flows at high Reynolds numbers: recent advances and key issues. *Phys. Fluids* **22**, 065103.

MATHIS, R., HUTCHINS, N. & MARUSIC, I. 2009 Large-scale amplitude modulation of the small-scale structures in turbulent boudnary layers. *J. Fluid. Mech.* **628**, 311–337.

MATHIS, R., MARUSIC, I., CHERNYSHENKO, S. I. & HUTCHINS, N. 2013 Estimating wall-shear-stress fluctuations given an outer region input. *J. Fluid. Mech.* **715**, 163–180.

METZGER, M. M. & KLEWICKI, J. C. 2001 A comparative study of near-wall turbulence in high and low Reynolds number boundary layers. *Phys. Fluids* **13**, 692–701.

MOSER, R. D., KIM, J. & MANSOUR, N. N. 1999 Direct numerical simulation of turbulent channel flow up to $Re_\tau = 590$. *Phys. Fluids* **11**, 943–945.

ORLANDI, P. & JIMENEZ, J. 1994 On the generation of turbulent wall friction. *Phys. Fluids* **6**, 634–641.

PARK, J., HWANG, Y. & COSSU, C. 2011 On the stability of large-scale streaks in the turbulent Couette and Poiseulle flows. *C. R. Méc.* **339** (1), 1–5.

PERRY, A. E. & CHONG, M. S. 1982 On the mechanism of turbulence. *J. Fluid Mech.* **119**, 173–217.

PERRY, A. E., HENBEST, S. & CHONG, M. S. 1986 A theoretical and experimental study of wall turbulence. *J. Fluid Mech.* **165**, 163–199.

PUJALS, G., GARCÍA-VILLALBA, M., COSSU, C. & DEPARDON, S. 2009 A note on optimal transient growth in turbulent channel flows. *Phys. Fluids* **21**, 015109.

RICCO, P. & QUADRIO, M. 2008 Wall-oscillation conditions for drag reduction in turbulent channel flow. *Intl J. Heat Fluid Flow* **29** (4), 891–902.

SAIKRISHNAN, N., DE ANGELIS, E., LONGMIRE, E. K., MARUSIC, I., CASCIOLA, C. M. & PIVA, R. 2012 Reynolds number effects on scale energy balance in wall turbulence. *Phys. Fluids* **23**, 015101.

SCHMID, P. J. & HENNINGSON, D. S. 2001 *Stability and Transition in Shear Flows*. Springer.

SCHOPPA, S. & HUSSAIN, F. 1998 A large-scale control strategy for drag reduction in turbulent boundary layers. *Phys. Fluids* **10**, 1049–1051.

SCHOPPA, W. & HUSSAIN, F. 2002 Coherent structure generation in near-wall turbulence. *J. Fluid Mech.* **453**, 57–108.

SMITH, J. R. & METZLER, S. P. 1983 The characteristics of low-speed streaks in the near-wall region of a turbulent boundary layer. *J. Fluid Mech.* **129**, 27–54.

TOH, S. & ITANO, T. 2005 Interaction between a large-scale structure and near-wall structures in channel flow. *J. Fluid Mech.* **524**, 249–262.

TOMKINS, C. D. & ADRIAN, R. J. 2003 Spanwise structure and scale growth in turbulent boundary layers. *J. Fluid Mech.* **490**, 37–74.

TOMKINS, C. D. & ADRIAN, R. J. 2005 Energetic spanwise modes in the logarithmic layer of a turbulent boundary layer. *J. Fluid Mech.* **545**, 141–162.

TOUBER, E. & LESCHZINER, M. A. 2012 Near-wall streak modification by spanwise oscillatory wall motion and drag-reduction mechanisms. *J. Fluid Mech.* **693**, 150–200.

TOWNSEND, A. 1976 *The Structure of Turbulent Shear Flow*. Cambridge University Press.

WALEFFE, F. 1997 On a self-sustaining process in shear flows. *Phys. Fluids* **9**, 883–900.

WALEFFE, F. 1998 Three-dimensional coherent states in plane shear flows. *Phys. Rev. Lett.* **81**, 4140–4143.

WALEFFE, F. 2001 Exact coherent structures in channel flow. *J. Fluid Mech.* **435**, 93–102.

WALEFFE, F. 2003 Homotopy of exact coherent structures in plane shear flows. *Phys. Fluids* **15**, 1517–1534.

WEDIN, H. & KERSWELL, R. R. 2004 Exact coherent structures in pipe flow: travelling wave solutions. *J. Fluid Mech.* **508**, 333–371.

WILLIS, A. P., HWANG, Y. & COSSU, C. 2010 Optimally amplified large-scale streaks and drag reduction in the turbulent pipe flow. *Phys. Rev.* E **82**, 036321.